24th INTERNATIONAL CONGRESS ON SOUND AND VIBRATION
23–27 July 2017, London

MEASURING MODAL DAMPING OF A MULTIBODY SYSTEM WITH DRY FRICTION

Balint Magyar, Roland Zana, Richard Wohlfart, Gabor Csernak and Gabor Stepan

Budapest University of Technology and Economics, Department of Applied Mechanics, Budapest, Hungary
email: magyar@mm.bme.hu

In metal cutting, the damping of the machine-tool-workpiece loop plays a key role in the stability of the process, particularly in case of high speed machining. A relevant part of structural damping originates in dry friction. This paper presents measurement results aiming to distinguish material damping from the damping related to the dry friction between the conforming surfaces of the assembled machine parts. Two discs had been manufactured, one of the discs is monolithic, the other one consists of two shrink-fitted bodies. The shrink-fitted disc has the same geometry as the monolithic one, and the overlap of the shrink-fitting was designed to obtain a contact pressure distribution that lies in the same order of magnitude as it appears in the spindle-tool holder connection. Free vibration decays had been measured on both discs. Significant differences were experienced in the decay ratios between the solid disc and the shrink-fitted one in some of the mode shapes. The obtained results can provide reliable basis for friction models in forthcoming finite element solvers.

Keywords: modal damping, decay, dry friction

1. Introduction

Modal analysis of monolithic structures by using finite element method currently belongs to routine tasks even in the industry. However, in case of assemblies, there is no off-the-shelf solution, see e.g. [1] and [2]. On the one hand, there is the uncertainty of the contact stiffness, on the other hand the modelling of dry friction-related damping is extremely challenging. In metal cutting the damping of the machine-tool-workpiece loop plays a key role in the stability of the process, particularly in case of high speed machining [3], [4], and a relevant part of structural damping originates in dry friction.

In this paper, measurement results are presented, which can be used to validate friction models in forthcoming finite element solvers. Two test-specimens had been designed and manufactured. One of the specimens is monolithic, the other one consists of two shrink-fitted parts. The shrink-fitted disc has the same geometry as the monolithic one, and the overlap of the shrink-fitting was designed to obtain a contact pressure distribution that lies in the same order of magnitude as it appears in the spindle-tool holder connection.

An automated pneumatic ball shooter was used for the excitation to ensure the initial conditions to be as identical as possible. Vibrations had been measured by laser Doppler vibrometers and lightweight accelerometers as well. Short-time Fourier transform was applied on the acquired velocity and acceleration signals, and characteristic amplitude peaks had been traced during the decays. The modal analysis of the monolithic disc had been carried out by using finite element method, and the traced peaks were selected based on the finite element results.

2. Test specimens

2.1 Design criteria

The test specimens had been designed to be suitable for free vibration decay experiments and forced vibration experiments by using an available electrodynamic shaker. In order to achieve higher amplitudes on a shaker, the weight of the specimens was kept reasonably small, and to exploit the optimal frequency ranges of the accelerometers and laser Doppler micrometers, natural frequencies were tuned to the preferred 300 Hz - 3 kHz range.

Since the only feasible approach of the finite element modelling of vibrating assemblies with dry friction is the use of full transient solution, it is an excessively intensive task from computational view-point. Consequently, a geometry modelled with 2D finite elements is beneficial. Thus, the mode shapes in question must be planar or axisymmetric. Moreover, well-defined contact surfaces and pressure distributions are preferred: threads should be avoided because of their relatively complex geometry, and shrink-fit is preferred to provide prestress.

2.2 Geometry

The half-sections of the realized specimen geometries are shown in Figure **1**. In case of the specimen that consists of two bodies (Figure **1**, right panel), the overlap of the shrink-fitted cylindrical surfaces is 0.03 mm in diameter, and the magnitude of the calculated prestress on the contacting surfaces varies between 10 and 40 MPa. The outer part was heated to 180 °C prior to the shrink-fitting. After the assembly, the two specimens were adjusted on an ultra precision milling machine, hence ensuring that the two discs are as identical as possible.

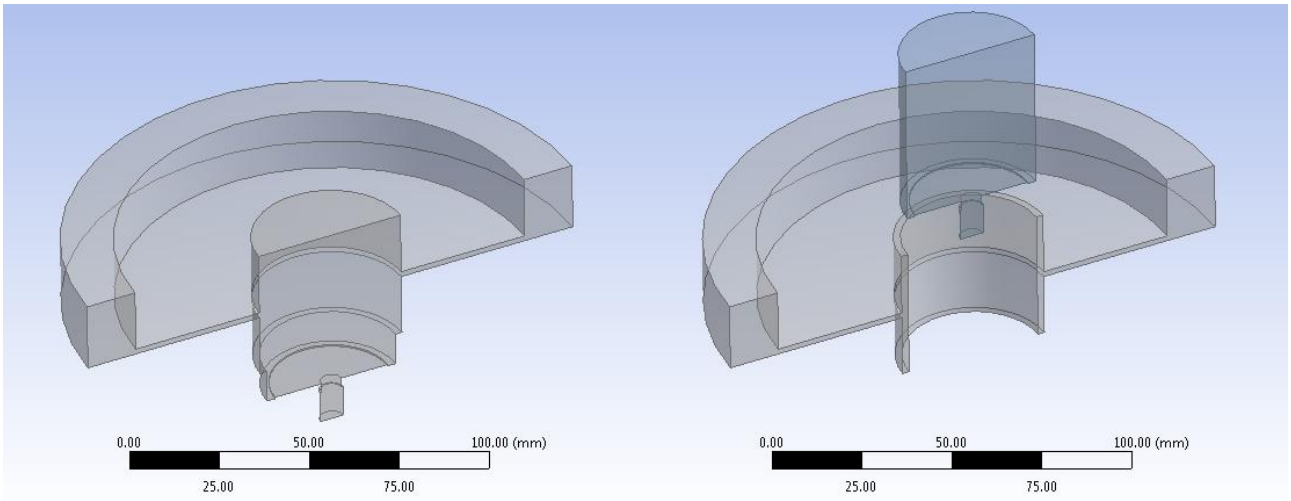

Figure 1: Half-sections of the test specimen geometries, left: monolithic, right: shrink fitted assembly.

2.3 Modal analysis of the monolithic disc

In order to identify mode shapes and natural frequencies of the test specimens, modal analysis was carried out by using ANSYS finite element software and 3D solid elements. Figure 2 presents the result regarding the monolithic disc.

The natural frequency of the first mode is 524 Hz, and this mode corresponds to the translational motion of the outer rim opposite to the inner core. This mode can be simulated in a 2D analysis as an axisymmetric problem. The second natural frequency is 729 Hz, which belongs to the tilting motion of the rim. This frequency appears twice due to the slightly perturbed cylindrical symmetry. The third natural frequency is 2366 Hz, and it corresponds to the bending vibration of the outer rim. It is a duplex mode as well, just like the fourth one at 5605 Hz, which corresponds to the bending vibrations of the thin membrane between the core and the rim.

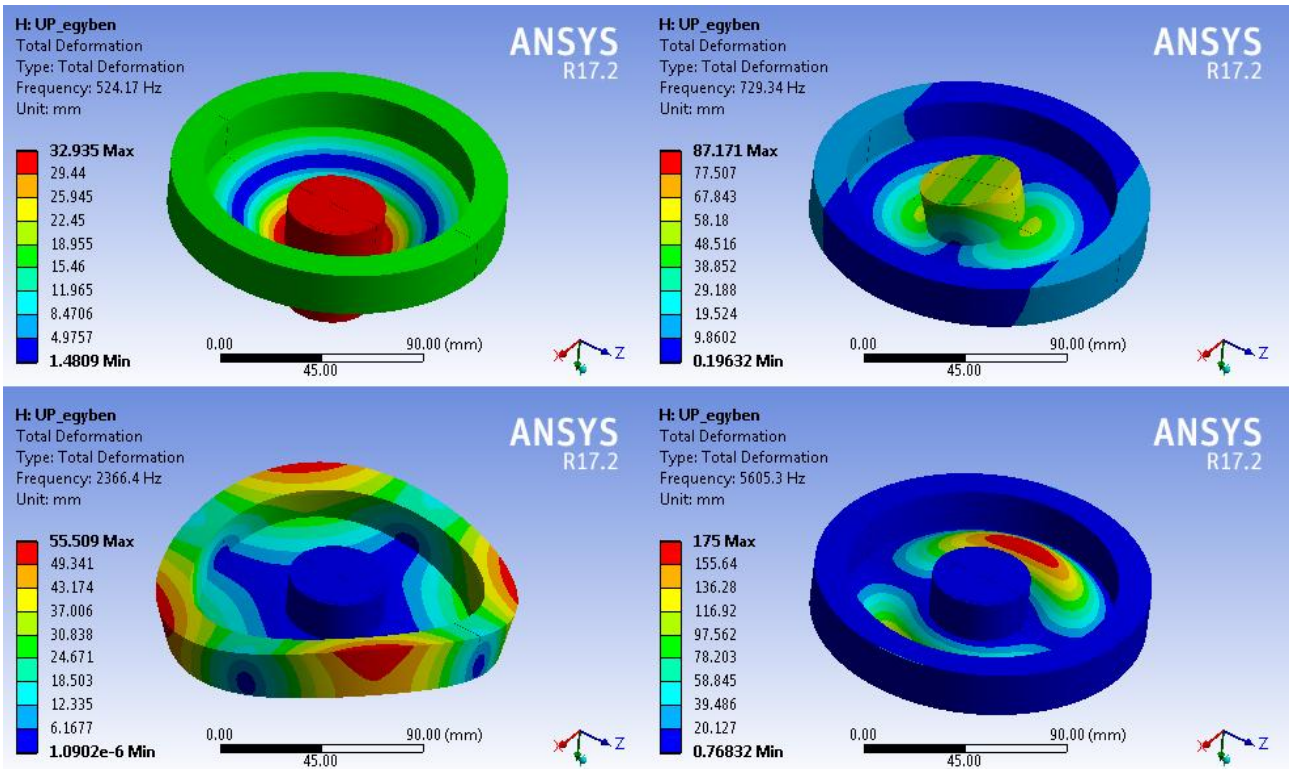

Figure 2: Natural frequencies and mode shapes of monolithic disc.

3. Laser Doppler vibrometers

Since the aim of the experiment is to quantify damping, non-contact devices, like laser Doppler vibrometers (LDVs) were preferred in order to avoid the increase of damping and/or mass. These vibrometers were used in two different measurements setups. First, forced vibration experiments were performed by using an electrodynamic shaker. Unfortunately, the power of the shaker was not sufficient, and at frequencies close to resonance (520-530 Hz) the vibration amplitude of the disc core was not in detectable range of the LDVs. After that, an experiment was performed with suspended specimens, but the LDVs were not usable in this case either because of the large-amplitude swinging motion.

4. Ultralight accelerometers

After the experiences with contactless vibrometers, ultralight MEMS based accelerometers were tested (Xtrinsic FXLN8361QR1). These accelerometers were mounted on a printed circuit board (PCB), and the power supply was also constructed.

Figure 3: Left: ultralight accelerometer, power supply. Right: calibration of the accelerometers.

The total weight of the accelerometer with the PCB was 0.065 grams, and the wire diameters were 0.08 mm. Compared to the 1720 grams of a disc, both the stiffness of the wires and the mass of the sensors could be neglected.

4.1 Calibration with Brüel & Kjær accelerometers

The product sheet of the Xtrinsic sensors specified 2.7 kHz as the upper frequency limit, therefore the calibration of these sensors was necessary. Two Xtrinsic sensors were placed on an electrodynamic shaker with a Brüel & Kjær DeltaTron Type 4397 accelerometer as a reference for the calibration. The shaker was driven with an exponential chirp signal from 10 Hz to 10 kHz, and the three channels were recorded with a sampling frequency of 100 kHz.

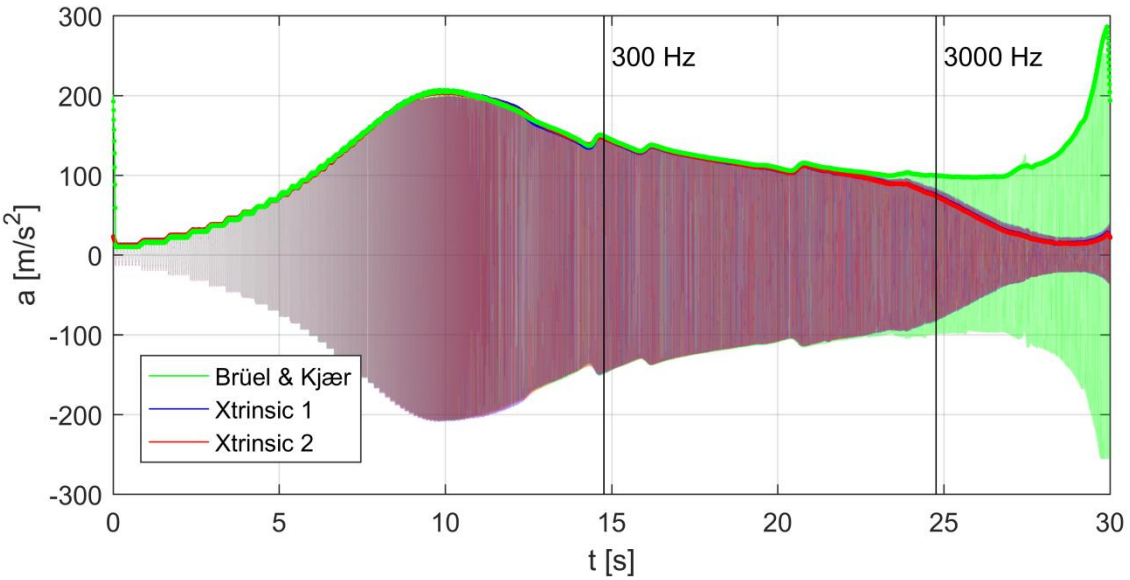

Figure 4: Calibration of the MEMS based accelerometer.

The time signal (thin curves) together with the RMS $\times\sqrt{2}$ values (thick curves) are presented in Figure 4, and the ratio of the Brüel & Kjær and Xtrinsic RMS values are shown in Figure 5 in the 300 Hz - 3 kHz frequency range. A low pass FIR filter was created with a cut-off frequency of 3 kHz, and the frequency response of the filter was adjusted to the fitted curve in Figure 5, hence compensating the inaccuracies of the Xtrinsic sensors.

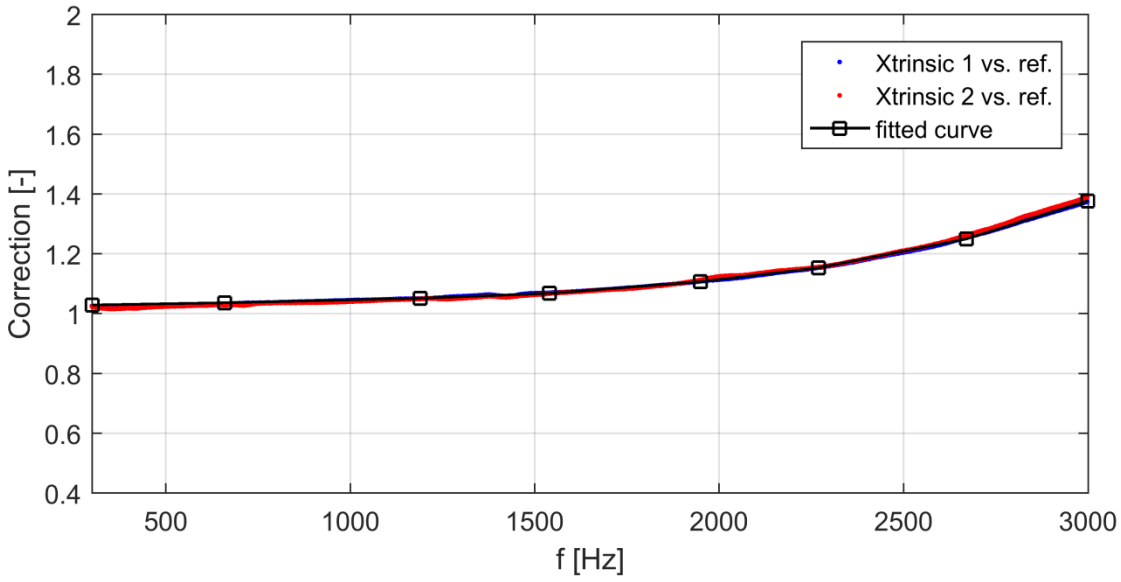

Figure 5: Ratio of the Brüel & Kjær and Xtrinsic RMS values.

5. Free vibration decay measurements

5.1 Measurement setup

Free vibration decays had been measured on both the monolithic and the shrink-fitted discs. The discs were drilled through the rims at ±60° relative to the top quadrant point, and suspended with kevlar fishing lines. An automated pneumatic ball shooter was used for the excitation to ensure the initial conditions to be as identical as possible. The places of impacts were at the top quadrant point of the rim. Two Xtrinsic accelerometers were placed at +90° and −120° relative to the shooting point, as shown in Figure 6.

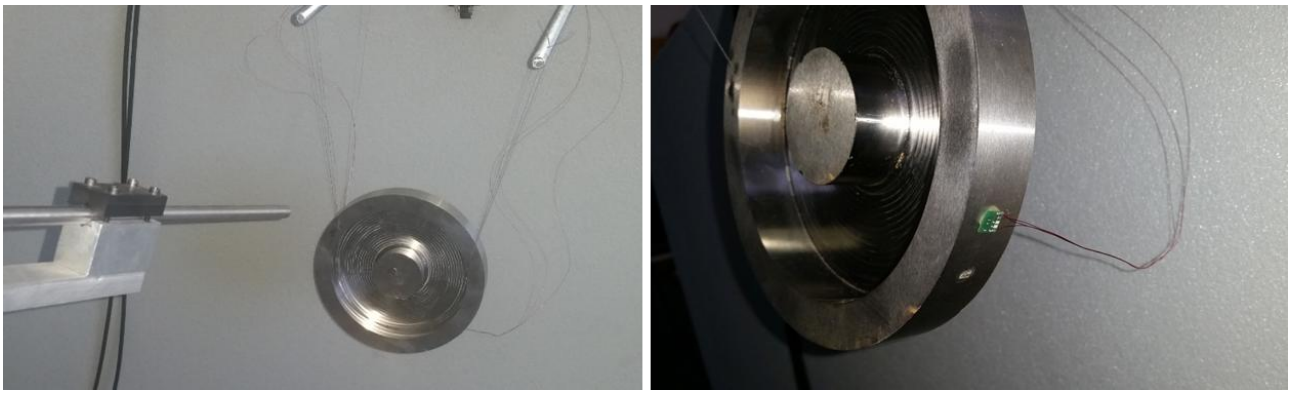

Figure 6: Left: suspended disc, automated pneumatic ball shooter. Right: Xtrinsic accelerometer attached on the side of the rim.

5.2 Evaluating the results

The accelerometer signals were recorded with 100 kHz sampling frequency. The free vibration decay time signals are shown in Figure 7. The difference in the decays can be clearly seen between the monolithic and the shrink-fitted disc.

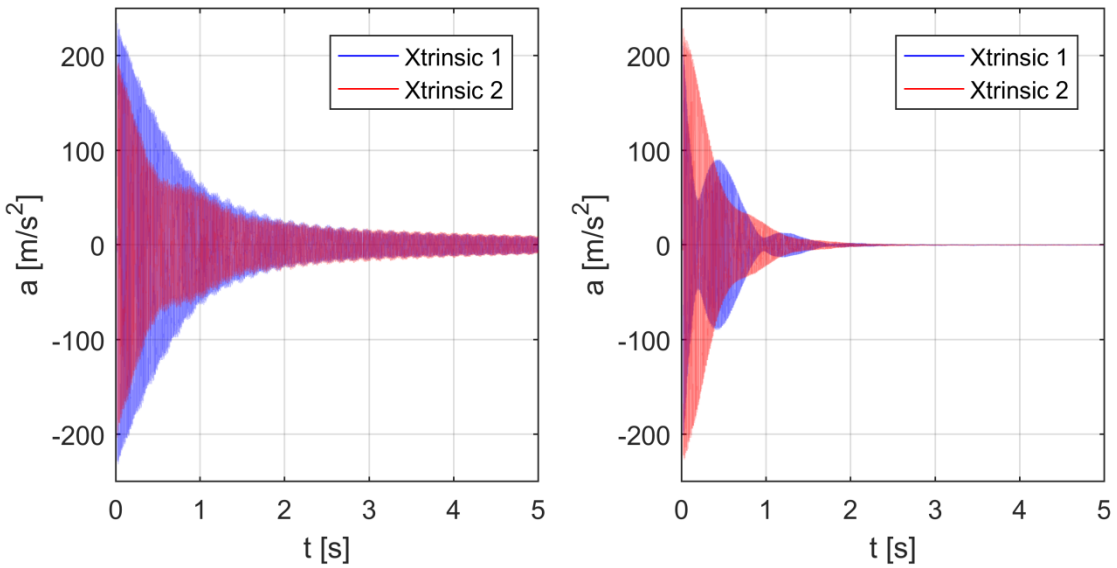

Figure 7: Free vibration decays. Left: monolithic disc, right: shrink-fitted assembly.

In order to identify the natural frequencies, fast Fourier transform (FFT) of the two decays were calculated on 5s samples as illustrated in Figure 8. The identified frequencies in case of the monolithic disc were in good accordance with the FEM results; moreover, there were no significant dif-

ferences either with the frequency peaks of the shrink-fitted disc compared to the FEA results with the monolithic disc. These frequencies are listed in the legend of Figure 9. Due to the imperfections of the manufacturing, the duplex frequencies are separated somewhat more than the FEA predicted ones.

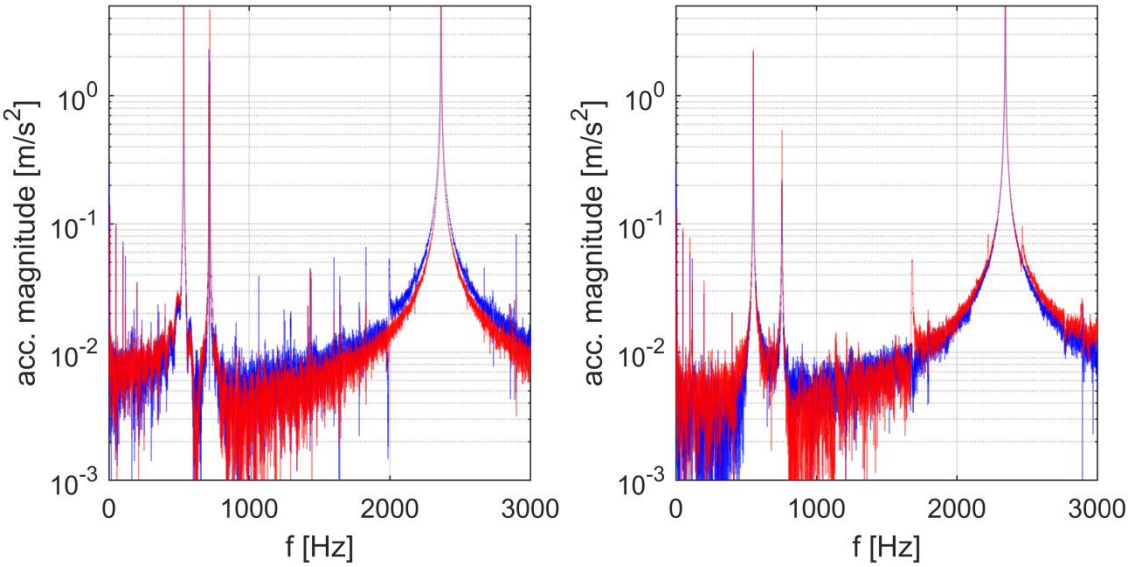

Figure 8: Frequency contents of the decays. Left: monolithic disc, right: shrink-fitted assembly.

In Figure 9, the decays of the acceleration magnitudes are shown; each curve corresponds to the average of 10 shots. A 0.25 s wide Blackman-Harris window was used for the short-time Fourier transform with a window overlap of 95%.

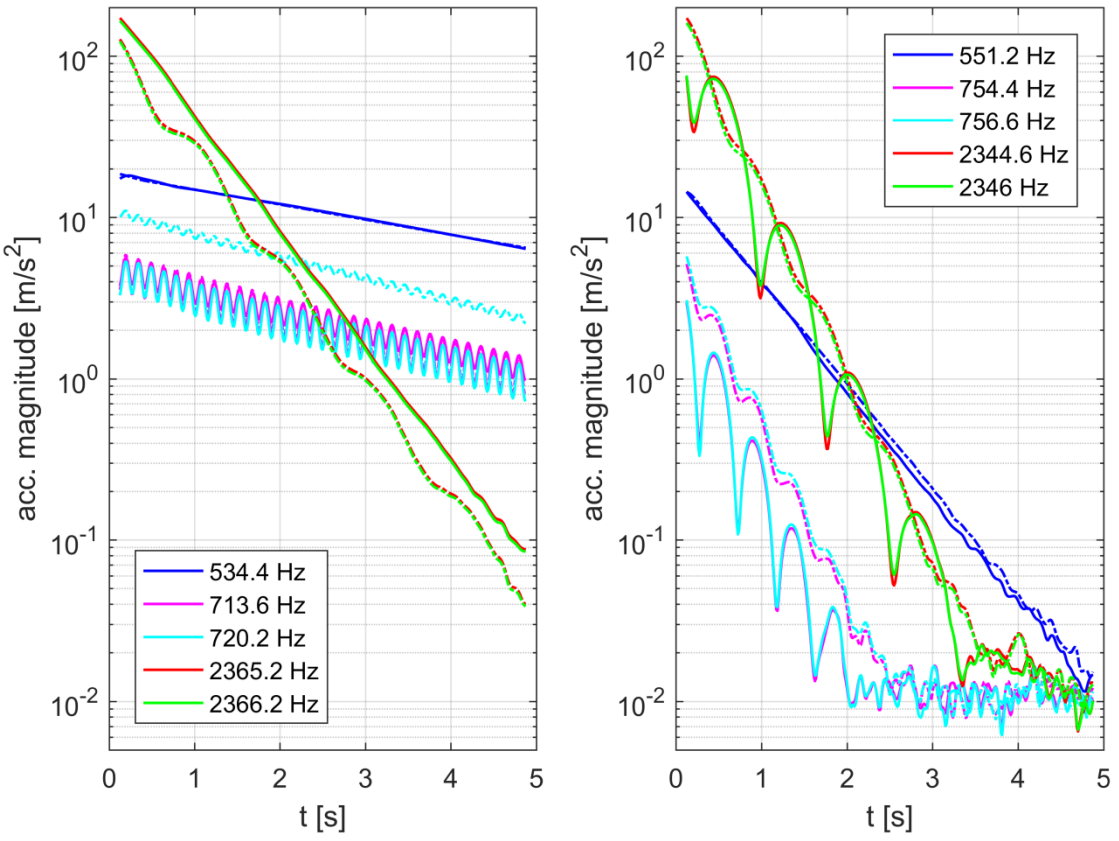

Figure 9: Free vibration decays of the acceleration magnitude peaks. Left: monolithic disc, right: shrink-fitted assembly.

In these charts, solid line corresponds to Xtrinsic 1 sensor, dashed line to Xtrisic 2 sensor. Each colour belongs to different acceleration magnitude peaks, i.e., vibration modes. Except for the decays denoted by blue colour, beat phenomena occur due to the relatively close natural frequencies, and beat frequencies are in accordance with the differences of the frequency pairs. The first mode shape has no symmetric counterpart, therefore there is no beat phenomenon there.

6. Conclusions

According to Figure 9, a significant difference was experienced in the decay ratios between the monolithic disc and the shrink-fitted assembly, which cannot be explained by the differences in material damping or air resistance, since both the material properties and the macroscopic geometry were identical of the specimens. Thus, it is possible to adjust material damping coefficients in a finite element simulation according to the measurement results corresponding the monolithic disc, and then, friction models and parameters can be adjusted to fit the decay ratios of the shrink-fitted disc's experiment.

7. Acknowledgement

The research leading to these results has received funding from the European Research Council under the European Union’s Seventh Framework Programme (FP/2007-2013) / ERC Advanced Grant Agreement n. 340889.

REFERENCES

1 Lazan B. J., *Damping of materials and members in structural mechanics*, Oxford: Pergamon Press; (1968).

2 De Silva C. W. Ed., *Vibration damping, control and design*, CRC Press; (2007).

3 Tobias S. A., *Machine tool vibration*, London: J. Wiley; (1965).

4 Stépán G., *Delay-differential equation models for machine tool chatter*, Dynamics and Chaos in Manufacturing Processes (1988); 471152935:165-192.

5 Smith J. O., *Spectral Audio Signal Processing*, W3K Publishing, (2011), ISBN 978-0-9745607-3-1.